Journal of Hydraulic Research Vol. 52, No. 4 (2014), pp. 532–544
http://dx.doi.org/10.1080/00221686.2014.912685

Research paper

Hydrodynamics and sediment transport in an estuary with an abrupt depth step

MARIANA G. PEREYRA, Postdoctoral Fellow, *Grupo Flujos Geofísicos y Ambientales, CIFICEN (CONICET – Universidad Nacional del Centro de la Provincia de Buenos Aires), Pinto 399, 7000 Tandil, Argentina*
Email: pereyramari@gmail.com

BEATRIZ M. MARINO (IAHR MEMBER), Research Professor, *Grupo Flujos Geofísicos y Ambientales, CIFICEN (CONICET – Universidad Nacional del Centro de la Provincia de Buenos Aires), Pinto 399, 7000 Tandil, Argentina*
Email: bmarino@exa.unicen.edu.ar

RICARDO N. SZUPIANY, Research Professor, *Facultad de Ingeniería y Ciencias Hídricas, Centro Internacional de Estudios de Grandes Ríos, Universidad Nacional del Litoral, C.C. 217, 3000 Santa Fe, Argentina*
Email: rszupiany@yahoo.com.ar

LUIS P. THOMAS (IAHR MEMBER), Research Professor, *Grupo Flujos Geofísicos y Ambientales, CIFICEN (CONICET – Universidad Nacional del Centro de la Provincia de Buenos Aires), Pinto 399, 7000 Tandil, Argentina*
Email: lthomas@exa.unicen.edu.ar (author for correspondence)

ABSTRACT
The hydrodynamic patterns resulting from the combination of tide flow, riverine discharge and bathymetry and their effects on water circulation and sediment transport are studied to assess the impact of geomorphic changes in the Quequén Grande River estuary (Buenos Aires, Argentina). A depth step located at about 2 km from the sea, created by dredging to provide favourable navigational conditions in the harbour, induces different flow patterns in the deeper and shallow estuarine parts, creating an attractive system to study. The main purpose of this paper is to report key physical features of this water system and the results of detailed longitudinal and transverse measurements of velocity and backscatter intensity. The data reveal the selective settling of suspended sediments in the harbour and a net loss of sediments to the sea. The effects of local severe storms that cause an intense tidal intrusion and mixing as well as a stronger ebb flow and seiches are also described.

Keywords: Anthropogenic changes; estuaries; hydrodynamics; Quequén Grande; sediment transport; tidal flows

1 Introduction

Estuaries are among the most heavily studied coastal systems due to the variety of problems raised from dynamical, physical, chemical, sedimentological, biological and economic points of view. The estuary's shape and extension are changed by erosion, sediments accumulation and the effects caused by sea level variations (Nichols and Biggs 1985). The interaction between fresh and salt water generates characteristic circulations as a result of their different densities and the turbulent mixing processes due to the tides and winds. The wide salinity range and the small thermal amplitude give these systems distinctive features (Dyer 1997). The main difficulty of studying them is that the river discharge, the tidal range and the sediments distribution are variable; consequently, many estuaries never form stable systems and then, because of the nature of being unique environments, they are not comparable (Perillo 1995).

In recent times, human demands on estuarine areas have expanded in terms of their use for industry, agriculture, domestic housing, fish and shellfish farming, leisure and tourism. Estuaries also provide significant coastal wildlife habitats. All of these interests depend, to a greater or lesser degree, on the hydrodynamic and sediment transport processes. In addition, human activities have a wide range of implications on estuarine morphodynamics, the extent of the consequences and their mitigation being the key inputs to strategic management planning (Reeve and Karunarathna 2009). Thus, long-term (>1 year) morphological changes in estuaries, increasingly influenced by human activities (Bale *et al.* 2007, Syvitski and Saito 2007), are of great importance to ecosystem, economics and environmental

Received 22 July 2013; accepted 2 April 2014/Open for discussion until 29 February 2015.

ISSN 0022-1686 print/ISSN 1814-2079 online
http://www.tandfonline.com

management and, therefore, receive considerable attention (Yang *et al.* 2001, van der Wal *et al.* 2002, Blott *et al.* 2006, Pari *et al.* 2008).

In the present study, hydrodynamic characteristics illustrating the performance of Quequén Grande River estuary (QGRE hereinafter), one of the most important estuaries in Argentina, are obtained based on the information of bathymetric and hydrographic measurements, paying special attention to its morphology, the meteorological factors and harbour activities. This small estuary has experienced substantial man-made modifications in the last century (i.e. frequent dredging operations, the construction of embankments and two jetties) that have altered not only the morphology, but also the water circulation. As in many estuaries with deepwater ports, artificial dredging is important to maintain the navigation channels thus giving specific shapes to the bed. In this context, one of the specific features of QGRE is the formation of an abrupt depth step which separates the last 2 km of the estuary (where the harbour is installed) from the shallow part upstream of the step.

In spite of its strategic importance, few measurements and field observations of QGRE have been made. First, the Franzius Institute (1963) conducted a technical study of the harbour area for completely different conditions from currently existing. Wright (1968) initially reported the distributions of the grain size of the sediments concluding that sands, silty sands and silty clays constitute the bottom sediments along the thalweg with mean grain size decreasing inland. A statistical study and numerical modelling of the wave conditions at the mouth of the harbour to design the extension of the southern jetty was carried out by port authorities in 1988. Lanfredi *et al.* (1988) have studied the variations of the mean sea level in Quequén Harbour, analysing 64 years of hourly tidal heights, and obtained the positive long-term trend of 1.6 mm year^{-1}, which is in general agreement with similar variations worldwide. Preliminary studies on geomorphology, physical hydrography, water balance, hydrographic-pluviometric regime, agricultural use and socio-economic aspects in the basin of the Quequén Grande River were reviewed by Campo de Ferrera (1998) while a brief description of the general estuarine hydrography was given by Piccolo and Perillo (1999). Perillo *et al.* (2005) provided a review of the status of the geomorphology and main physical characteristics of the estuary and reported spatial distributions of salinity, temperature and velocity obtained during six surveys between April 1994 and August 1998. Their measurements were carried out before the remodelling and extension of the southern jetty completed in 2008. This work clearly indicated that a better understanding of the estuary morphology and hydrography is necessary to face and address the existing sediment-related problems. More recently, Isla *et al.* (2009) analysed the morphological changes of the neighbouring beaches formed before, during and after the extension of the southern jetty, and concluded that the effects induced by the river are not important under normal conditions. However, significant silting may take place during exceptionally high flood events. All these previous studies lack integration of morphological, hydraulic and sedimentological considerations due to limitations of methodologies and equipment employed in the past. The absence of systematically obtained quantitative information prevent the comparisons of the present estuarine characteristics to those prior to port dredging or remodelling of jetties.

The goal of this paper is to report the study of the dynamics of the tidal and riverine flows, which in combination generate a distinctive pattern of sediment accumulation in the harbour zone, in order to assess the impact of human interventions in a natural system. To achieve this, field measurements were performed with a high level of spatial and temporal resolution. In addition, evidence of the generation of standing waves after the occurrence of a severe local storm is given. A better understanding of both estuarine geomorphology and hydrography will certainly be useful to solve QGRE dredging problems with minimum negative effects to the environment.

2 Background

The Quequén Grande River is 173 km long, born in the Tandilia low mountain range and reaches the Argentinean Sea after crossing the Necochea-Quequén urban centre (Fig. 1a). It has a width that ranges between 150 and 200 m, a minimum thalweg depth of 1.80 m and an important number of tributaries organized in a dendritic pattern (Campo de Ferrera 1998). Its basin extends in a zone covering a total area of about 9900 km^2 in the southeast of Buenos Aires Province, in which the conditions to develop small falls and rapids along the river are favourable. The last minor falls, named Las Cascadas, are located at 17 km from the mouth (Fig. 1a), coinciding with the furthest point where the effects of the tide are detected, and therefore marking the head of the estuary according to the estuarine definition criteria proposed by Perillo (1995).

The climate is maritime temperate with rains diminishing progressively from east to west. The highest mean values of precipitation are registered between September and March in the range 57–100 mm/month while June, July and August are the months with the minimum mean values (36–50 mm/month). Mid-latitude westerly winds and the influence of the subtropical South Atlantic High dominate the typical weather pattern of the region. The resulting circulation induces strong north-west and north winds (Merlotto and Piccolo 2009). The more frequent winds are produced in the north-west (13.3%) and west (11.6%) directions, with velocities ranging from 5.6 to 8.3 m s^{-1}.

The river has a permanent but limited flow that ranges from 6 to 50 m^3 s^{-1} (with occasional maxima of about 170), measured monthly at the gauging station situated near Las Cascadas Falls. Occasional abundant rains generate flooding that temporarily changes the river flow. The measurements of pH indicate that the freshwater is alkaline (>8 all year) and oxygenated. The suspended particulate matter depends on the river flow variation and the duration and intensity of the rains. Suspended solids

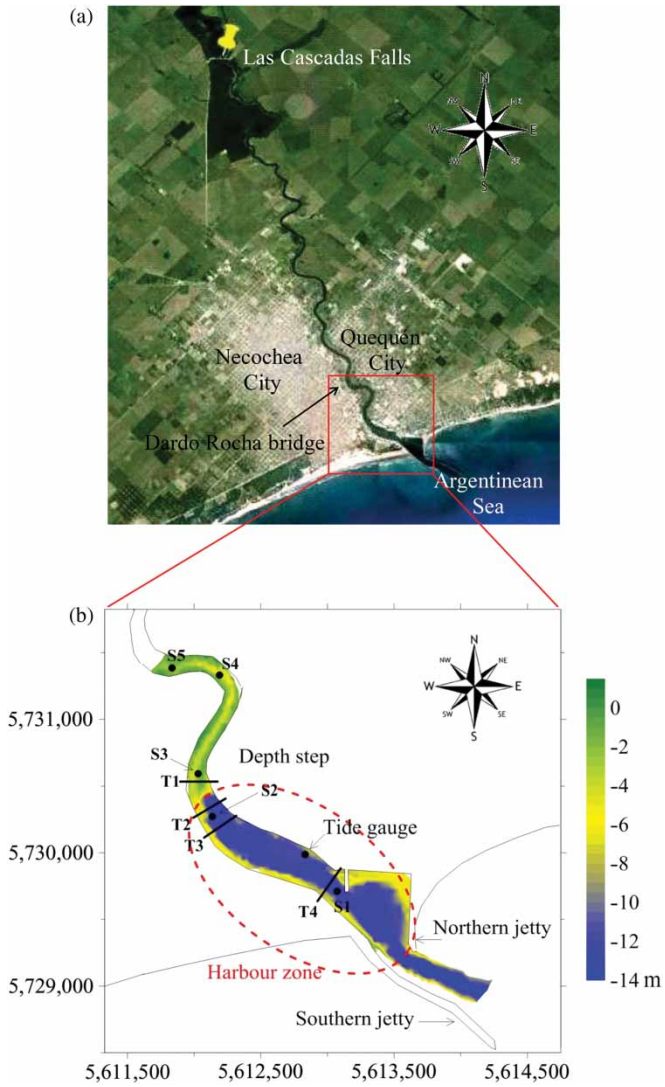

Figure 1 (a) Estuary head location. (b) Bathymetry of the last 3.7 km of QGRE together with the locations of measurement stations S1–S5 and transverse cross-sections T1–T4. Coordinates are given in metres according to Gauss–Kruger projection

concentration varies in the range of 40–1140 mg l^{-1} for river flows between 10 and 100 m^3 s^{-1}, respectively.

The Quequén Harbour is located in the last 2 km of the estuary, modifying the original morphology of the river mouth. It is the second largest seaport in Argentina, with activities related to the export of grains and oleaginous products coming from an extensive hinterland, imports of fertilizers, and coastal and inner shelf fisheries. The port has two protecting jetties, the recently extended southern one measuring 1192 m, and the northern one of 572 m (Fig. 1b). To provide adequate navigational conditions, the flow depth is kept to be 12 m within a width of 120 m by regular dredging. This part of the estuary is flat with a trapezoidal-shaped cross-section. Further upstream, the thalweg is 3–4 m deep, with an irregular topography exhibiting 5 m deep small canals formed by the currents. Thus, an artificial step that separates the estuary into two parts is generated. In the bathymetric map (Fig. 1b) it is also observed that the step is not perpendicular to the longitudinal direction of the estuary. The strong tendency of the suspended solids to be trapped at the foot of the step is the main cause of dredging to maintain the navigability in the harbour area. These parts of the estuary are affected by the tide in different ways. Hence, distinctive flow patterns downstream and upstream of the step are induced, while the reduced water circulation produces strong reductive and even anoxic conditions in the harbour zone that is permanently flooded by seawater.

The estuary is classified as a microtidal coastal plain primary system (Perillo *et al.* 2005), partly mixed from the step to the head, while in the harbour zone the water column is typically stratified. The upper 1–3 m layer of the water column is brackish water with a halocline below with salinities reaching over 30 practical salinity units (PSU), being homogeneous down to the bottom. The tide is mixed and predominantly semidiurnal with an annual mean range of about 1.0 m although it occasionally reaches 2.2 m. Four tidal constituents are significant, with the principal lunar semidiurnal M2 being the most important. Spectral analysis of the water height suggests that the sea level may be atmospherically forced on the adjacent shelf at macro-, synoptic and local scales (Dragani *et al.* 2002). Wave action along the coast is so high that the harbour does not provide adequate navigational conditions and must be closed many days a year. Before the enlargement of the southern jetty (by about 400 m) between 2004 and 2007, this occurred about 70 days a year when the waves exceeded a height of 1.8 m, while after that the periods of closure of the harbour was reduced to only 42 days a year when the waves exceeded a height of 2.4 m. Peak waves of the order of 5 m are common, especially during the typical south-eastern winds that hit the coast 5–10 times a year on average.

Very high flash floods have taken place sporadically during the last century among which the most important were registered in 1905, 1913, 1915, 1980, 1986, 1987, 1998, 2002 and 2012. According to Isla *et al.* (2009), the exceptional floods occur only during the years in which the *El Niño-Southern Oscillation* conditions develop, producing a significant transport of suspended sediments towards the sea.

As the deep part of the estuary is orientated about 60° to the north–south direction, this zone is susceptible to the action of NW–SE winds. The strongest winds come from the S–SW, occasionally exceeding 100 km h^{-1}, generating stronger tides and mixing in the estuary harbour zone. The occurrence of the locally important climatic phenomenon that consists of a sudden rotation of cold southern winds to the SE after blowing for some days can take place several times a year (Gan and Rao 1991). As seen later, during these events the water level offshore rises significantly, often producing flooding and water currents more intense than normal, driving the sea water upstream and causing standing waves. Additionally, as a consequence of storm surges, highest variations of about +1.5 and −1.70 m compared with the astronomical tide with a mean duration of 1 and 1½ days were reported for the period 1979–2006.

3 Methods and materials

Five measurement stations were set along the last 3.7 km of the estuary inside and near the harbour zone as indicated in Fig. 1b, being S2 the nearest to the depth step in the deeper part while S3–S5 are upstream of the depth step. The local tide gauge and weather stations (located inside the harbour) provide every 10 min the values of tide height and temperature, humidity, atmospheric pressure, wind speed and direction, respectively.

To characterize the kind of sediment swept by the river up to the harbour zone, samples of bottom sediments were collected with a small mesh net at sites located at 6, 19, 45 and 90 km from the sea, and between stations S1 and S2. The granulometric analysis was conducted with a particle analyser *Mastersizer* 2000 (*Malvern Instruments*) that employs laser diffraction and measures the relative concentration of particles between 0.02 and 2000 μm thus covering the required range. The distributions of the grain size indicate that nearly 50% of the sediments have a diameter between 30 and 300 μm with a maximum of about 90 μm with some seasonal variations. This suggests the predominance of very fine to fine sands and medium to coarse silt in the river, with gravel content being negligible.

Two surveys were carried out to obtain the information needed to characterize the QGRE hydrodynamics around the step and analyse its influence on the settling of the suspended matter. One of them, performed between 6 and 8 October 2008, took place after the occurrence of a severe wind storm. Strong south-easterly winds blew from midday the first day with increasing intensity up to a maximum of about 45 km h^{-1} at midnight (see Fig. 2a), causing an increase of the sea level and waves offshore higher than normal. The harbour was closed on 7 October thus contributing to the elimination of any perturbation on the measurements caused by the motion of ships. In the afternoon of the second day the wind speed diminished significantly and the wind changed direction to the north in the evening. A comparison between the tide level measured by the Port Authority mareograph and the astronomical tide due to gravitational force forecasted by the *Servicio de Hidrografía Naval* is presented in Fig. 2b. The tide was higher than the astronomical one while the south-easterly wind blew until noon of 7 October when the water height started to get close to the values of the tide tables. During the next day, while the northerly wind continued to blow, smaller tide height values than those forecasted prevailed. Longitudinal velocity and backscattering intensity measurements were performed between the Dardo Rocha Bridge (S5) and the pier (S1), moving at a constant velocity of 1.7 m s^{-1} along the axis of the estuary during several tidal cycles. A 600 kHz *Workhorse* acoustic Doppler current profiler (ADCP), provided by *Teledyne RD Instruments*, and a differential global positioning system were employed to obtain information about the velocity and backscatter intensity of the suspended matter and location, respectively. Salinity, temperature and density in the water columns at stations S1–S5 were also measured using a CTD (acronym for Conductivity, Temperature and Depth) *InterOcean*, Model 513E Portable. The CTD sensors measured water conductivity and temperature every 3 s with an accuracy of 0.05 m s cm^{-1} and 0.02 °C, respectively. The suspended sediments concentration was determined by measuring turbidity with a previously calibrated optical backscatter sensor attached to the CTD, ranging between 0 and 4000 NTU.

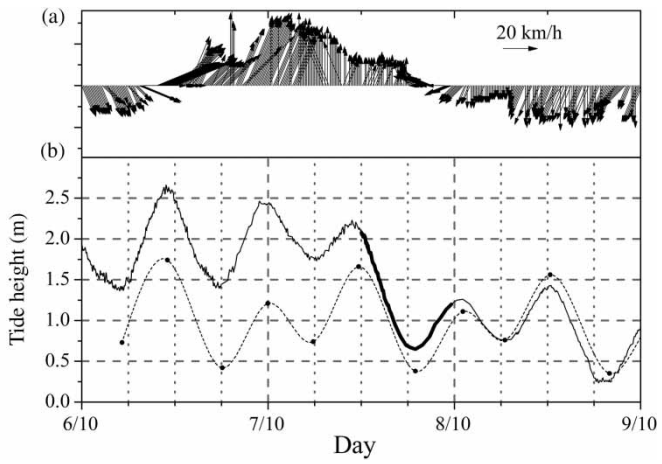

Figure 2 Correlation between (a) the wind speed (scale is indicated at top-right) and direction (arrows upwards represent south–north wind direction), and (b) the astronomical tide (dashed line) and the tide height measured by the mareograph (solid line). The thick solid line indicates the period during which the measurements reported in Figs. 3–6 were made. Data correspond to the field study on October 2008

On 9 and 10 April 2011 measurements were made across the estuary at the cross-sections T1 to T4 in Fig. 1b, during a complete cycle close to spring tide. Also several longitudinal cruises were performed from the sea up to S5 site. The prevailing quiet meteorological conditions in the previous days meant that the estuarine system was stratified when the surveys took place. To obtain transverse distributions of flow velocity and backscatter intensity, a 1200 kHz *Workhorse* ADCP was employed. Once all the measurement files were loaded, an exit file containing the information for two transverse cruises (depth, distance, velocity components, backscattering, Universal Transverse Mercator coordinates, etc.) was generated using the *Velocity Mapping Toolbox* application (Parsons *et al.* 2013). The ADCP used in our study has the maximum relative sensitivity for particles with a size of about 70 μm (Gartner 2004, Guerrero *et al.* 2011). Since the bottom sediments have a maximum concentration of grains with size ranging 80–100 μm, corresponding to a size close to the maximum sensitivity of the instrument, the backscatter intensity measured is appropriate to capture the motion of most suspended sediments.

4 Results

4.1 *Longitudinal distributions of velocity and backscatter intensity*

Figure 3a shows the longitudinal distributions of the velocity magnitude at the beginning of the ebb stage. Upstream of the

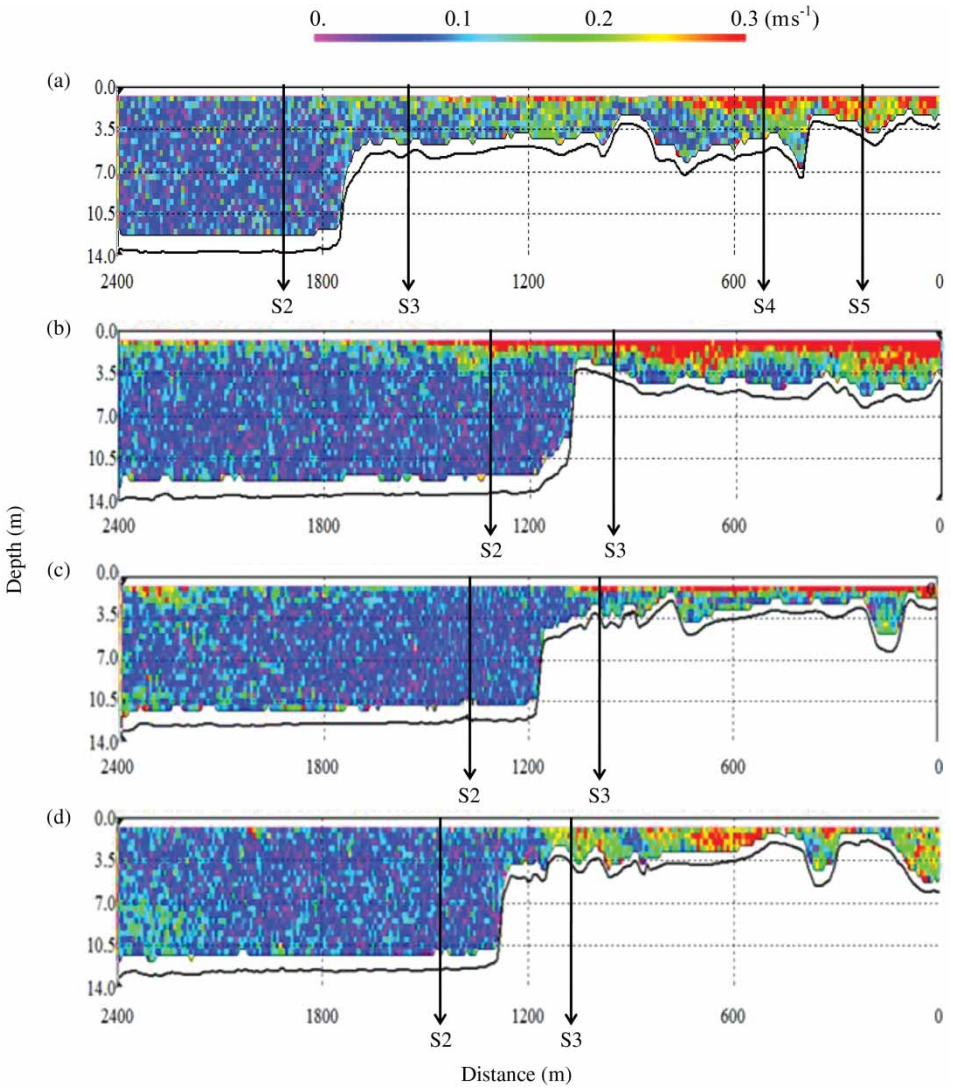

Figure 3 Distributions of velocity magnitude (in m s^{-1}) at (a) 12.30 h, (b) 13.30 h, (c) 19.37 h and (d) 22.25 h on 7 October 2008 (the position 0 m in abscissa corresponds to the point where a run starts)

step, the tide generates a continuous variation of the velocity from the bottom to the free surface where the maximum values are reached. The distribution obtained 1 h later (Fig. 3b) shows that this feature becomes more significant and a high-velocity surface layer forms in the harbour zone. At the end of this stage (Fig. 3c and 3d), the surface layer decelerates and becomes barely perceptible.

The measurements conducted at each of the stations S1–S5 are interpolated to obtain the vertical distributions of the longitudinal component of the velocity as a function of time shown in Fig. 4. An asymmetry of the current is visible for all stations. Particularly, the asymmetry at S2 may be understood considering that, during the ebb tide, the denser water remains at rest in the deep part of the estuary, while an upper layer of lighter fluid moves towards the sea. A careful inspection of the data suggests that the displacement of this surface layer seems to induce the formation of a weak, although extensive, vortex in the deeper layer of the harbour zone which we will return to in Section 5. In the estuarine shallow part (S3–S5) the velocity increases from the bottom towards the free surface according to that observed in Fig. 3a. During the ebb tide, the CTD measurements indicated the presence of a 1.7 m deep surface layer with salinity values ranging between 7 and 12 PSU, and temperatures about 3 °C higher than that of the deeper layers. The surface layer is formed by riverine freshwater mixed with salt water that was previously pushed upstream by the storm. Underneath this surface layer, unmixed sea water is found. As observed in the right-hand side of Fig. 4, during the flood tide, the velocity distribution is uniform at S2; upstream of the step (S3–S5), a surface current is first generated inland while a deep current moves in the opposite direction from approximately 18.00 to 20.30 h. After that, the velocity distribution becomes uniform over depth reaching a maximum shortly after 21.00 h at S4 and subsequently at S5. Although normal tidal heights generate less intense currents, this general behaviour of the estuarine flows was observed in all the surveys performed.

Figure 5a and 5b shows the backscatter intensity distributions of the suspended matter at the beginning of the ebb tide.

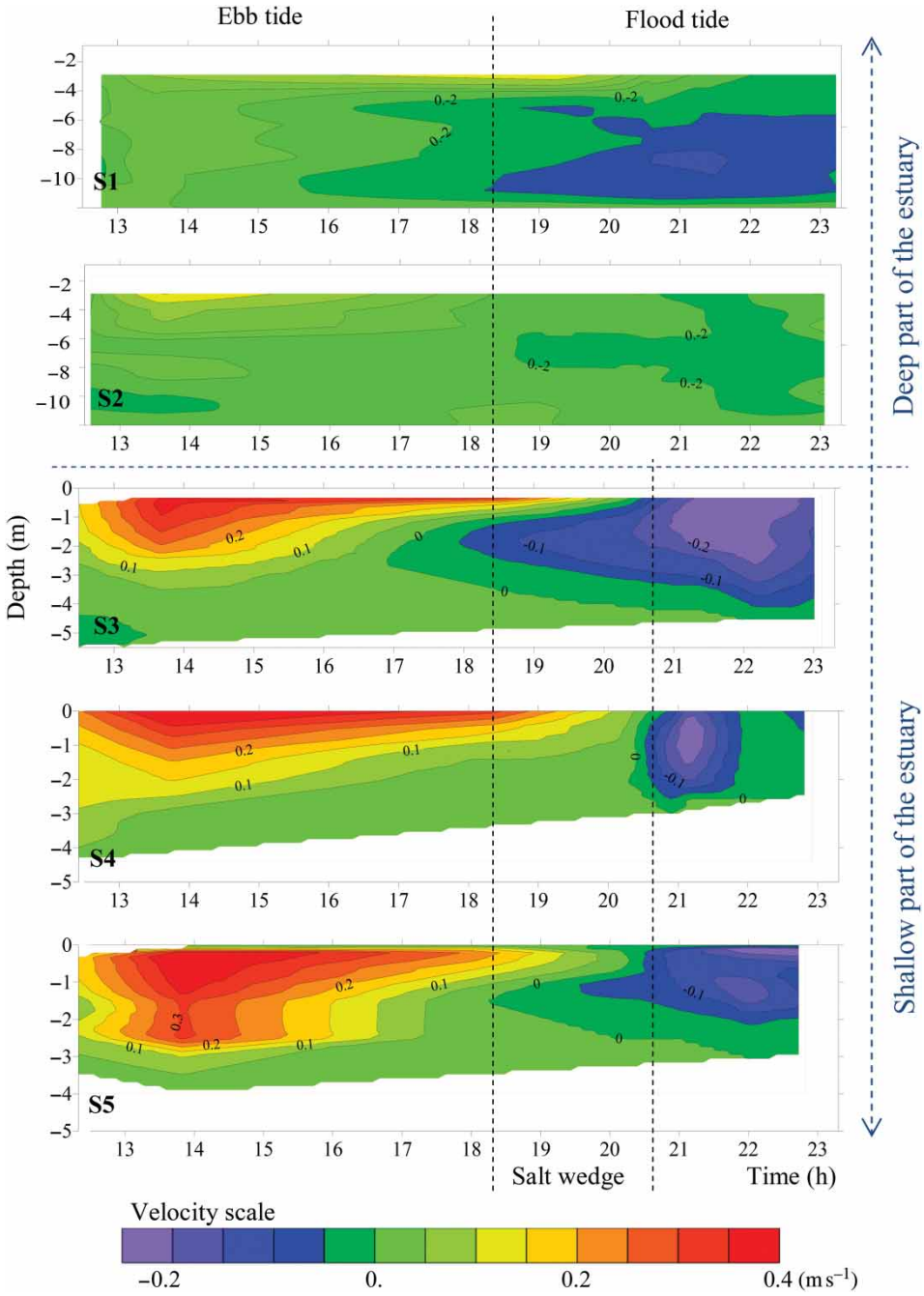

Figure 4 Distribution of the velocity longitudinal component (in m s^{-1}) measured over one tidal cycle in each station on 7 October 2008

There is a continuous increase of the sediment concentration from the bottom up to the free surface where maximum values are, in agreement with velocity distributions, as Fig. 5a shows. The sediments are transported in a surface layer to the deeper estuarine zone downstream. Figure 5b exhibits the distribution obtained 1 h later indicating that the sediment load becomes more noticeable with a thicker surface layer along the harbour zone; the sediments reach greater depths but do not cover the whole water column. The flow eventually stops at low water (Fig. 5c) and also ends the material transport to the harbour zone giving extra time for sediment settling. Sediments leave the upper layer and descend reasonably uniformly during this period. However, some convective instabilities (see explanation in Section 5.3) may be also seen in a number of places that convey sediments to the bottom quicker than the gravitational settling of individual particles. Figure 5d shows that most of the particles have settled in the period considered.

The activation of sediments due to the dredging operations and the motion of big bulk-carriers with consequent increase of the turbidity were observed by Pereyra (2013) in the harbour zone in a survey performed in December 2007. On that occasion, longitudinal measurements of velocity and backscatter intensity were made during the time at which a suction dredger (operating in the zone) went offshore to unload the sediments. It was found that after the dredging was completed the flow transported a great amount of suspended matter upstream during the flood phase

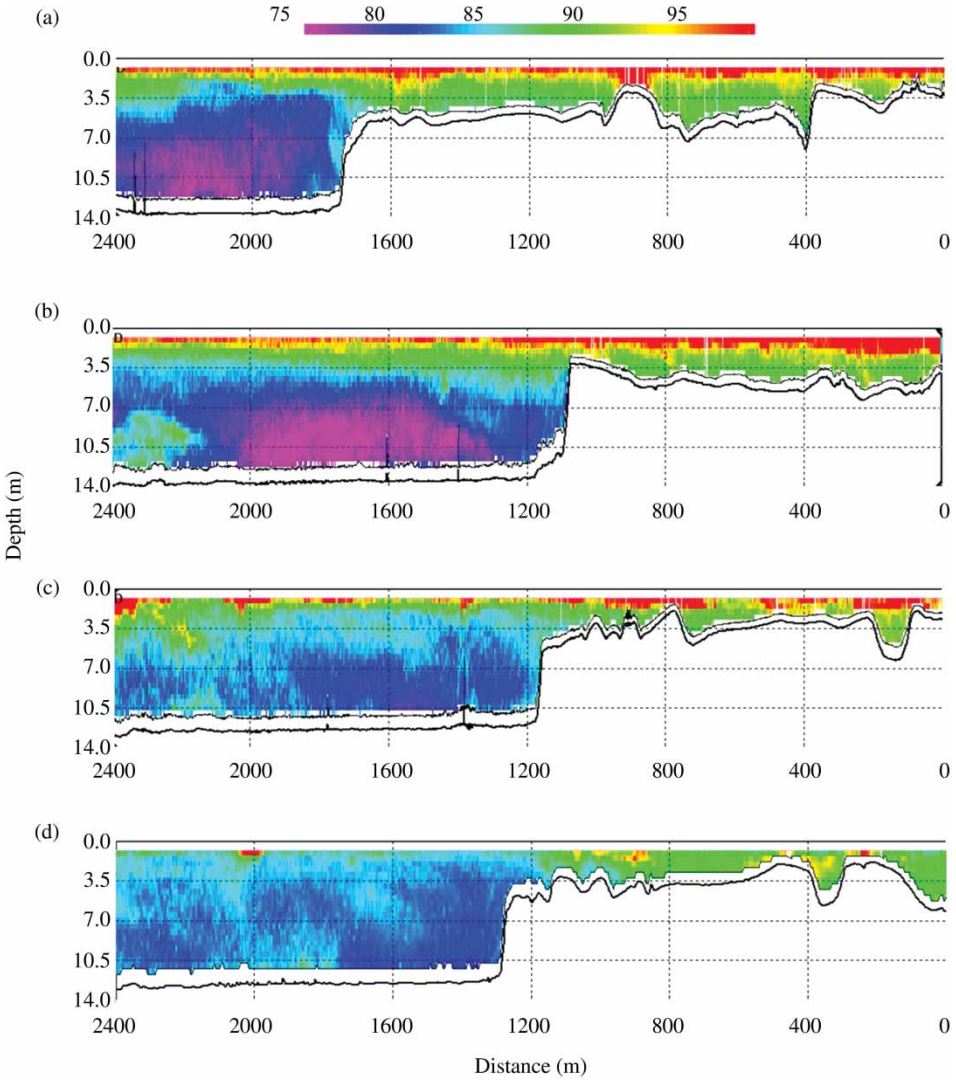

Figure 5 Backscatter intensity distributions (in dB) obtained at: (a) 12.30 h, (b) 13.30 h, (c) 19.37 h and (d) 22.25 h on 7 October 2008

of the tide, causing an important sediment redistribution in the estuary.

4.2 *Standing waves*

At midday of October 7 when the ebb tide started, a particular velocity distribution was found, shown in Fig. 6, indicating a succession of regions with north (magenta or red) and south (green) directions, and with the same intensity in the whole water column along the harbour zone. These features indicate the presence of shallow water waves propagating mainly in the north–south direction. To simplify the analysis, the northern component of the velocity was averaged over depth to obtain a relationship $u = u(x)$ where x is the position along the estuary. The inspection of the spatial change of the depth-averaged velocity u in Fig. 7 reveals a fundamental harmonic (dashed line) corresponding to a wavelength of the order of the harbour length, on which higher harmonics are superimposed. This is corroborated by the Fourier analysis that makes it possible to obtain the spectrum of key wave numbers contained in the velocity data. The alternative method employed here to obtain the main wave numbers is to calculate the best-fit function to $u(x)$ with the form

$$u = u_0 + u_1 \sin\left[\frac{2\pi(x - x_{c1})}{\lambda_1}\right] + u_2 \sin\left[\frac{2\pi(x - x_{c2})}{\lambda_2}\right] + \cdots \quad (1)$$

where u_i, x_{ci} and λ_i are the amplitude, phase and wavelength of the i-component of the series, respectively. The dashed line in Fig. 7a shows the first component of the velocity function approximation while Fig. 7b shows the second component calculated with the best-fitting process for $u^* = u - u_0 - u_1 \sin[2\pi(x - x_{c1})/\lambda_1]$.

The wave theory in the shallow water approximation (Whitham 1974) indicates that the amplitude of the velocity u_i is related to the height amplitude η_i of the wave i-component as

$$\eta_i = \sqrt{\frac{H}{g}} u_i \quad (2)$$

where H is the total local height from the bottom. Thus, if $H = 12$ m, it is found that the maximum velocity amplitude

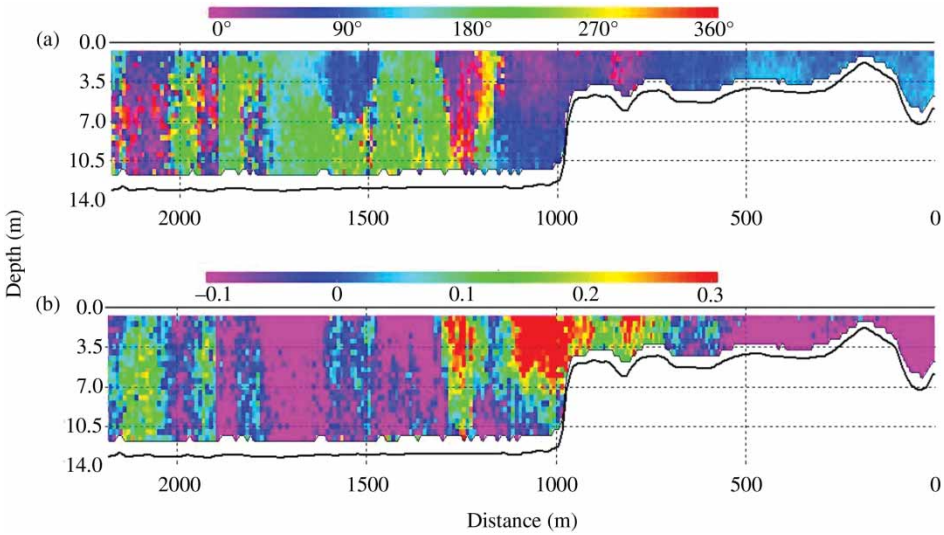

Figure 6 Distributions of the (a) velocity direction (0° and 360° indicate the north), and (b) velocity magnitude (m s^{-1}) of the northern component at the midday 7 October 2008 survey

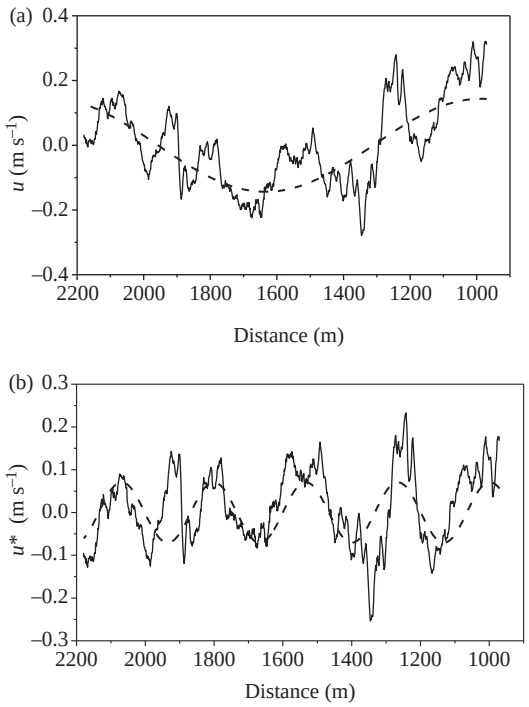

Figure 7 (a) Northern component of the depth-averaged water velocity (solid line) obtained from Fig. 6. The dashed line represents the best-fit sine function of the largest wavelength λ_1. (b) Second largest component (dashed line). The distance to the sea is represented in the horizontal axis (1000 m correspond to the depth step location according to Fig. 6)

$u_i \approx 0.3$ m s^{-1} corresponds to a maximum height amplitude $\eta_i \approx 0.3$ m. The features of these standing waves resemble those of several high-amplitude oscillations reported by Perillo *et al.* (2005), the cause of which was unexplained.

The results found for the first and second wave components by the best-fit approach suggest that the wave amplitude ranges from 0.10 to 0.30 m and the wavelength is about 2500 m. Similar values were found by the other surveys performed during the tidal cycle considered. These wavelength values are of the order of the distance between the depth step and the estuary's mouth, i.e. the length of the harbour zone. The generation of this kind of waves in QGRE will be explained in Section 5.

4.3 *Transverse distributions of velocity and backscatter intensity*

Measurements made in the cross-sections T1–T4 (indicated in Fig. 1b) add information about the general evolution of the estuarine circulation and sediments transport. At quiet meteorological conditions, during the tidal flood phase the flow was uniform throughout all cross-sections, being weak in the harbour zone and more intense in the shallow one since the cross-section is smaller there. At the beginning of the ebb tide, the flow is not spatially uniform. Figure 8 illustrates the velocity and backscatter intensity distributions obtained in the four cross-sections within a short period of time during the ebb tide. In the shallow part of the estuary (Fig. 8a), the high flow velocity enhances the bed shear stress leading to sediments erosion and re-suspension, as may be inferred from the stronger backscatter values. Figure 8b shows an intensification of the flow on the south-west side of T2 due to the presence of the bend. In the harbour area and far from the step (Fig. 8c and 8d), two layers with different velocities but with the same directions are developed: a thin and faster surface layer of brackish water and a deeper and slower thick layer of sea water. The brackish water layer thickness is similar to the depth at the crest of the step.

The sediments are transported from the shallow part of the estuary to the deeper harbour zone in the surface layer. At slack tide, the suspended matter transport ceases and the lower backscatter signal suggests that the settling takes place mainly in the harbour. Particularly, the sediments concentrate at the SW side near the step where major dredging is needed. When the flood phase starts again, most of the suspended solids already settled and the flow velocity is too low for the sediments to be

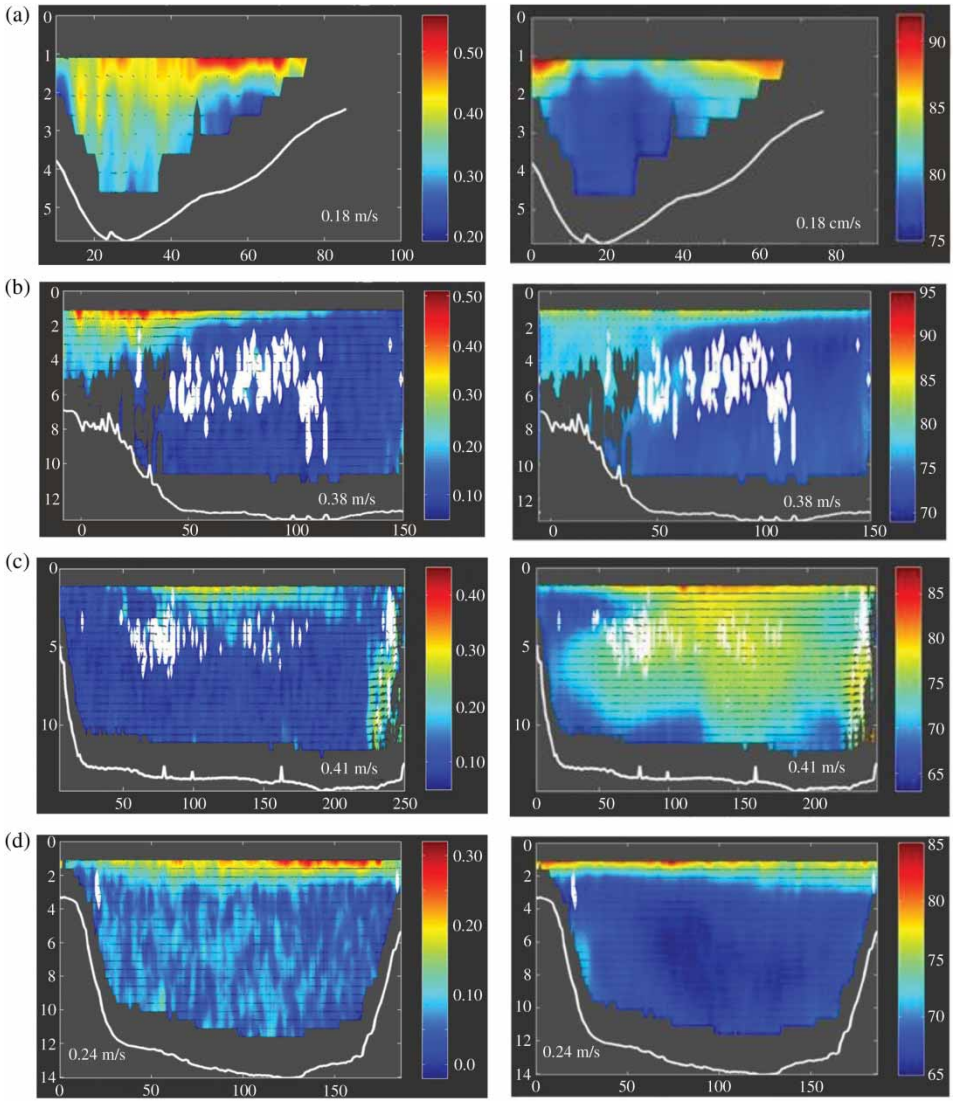

Figure 8 Transverse distributions of the longitudinal component of velocity (ms^{-1}) (left) and backscatter intensity (dB) (right) obtained at about 01:00 on 10 April 2011 during the ebb tide in the cross-sections (a) T1, (b) T2, (c) T3 and (d) T4. Axis numbers are given in meters.

transported upstream of the step. Thus, the particles are mainly deposited on the harbour bed. In the cross-section T4, the velocity distributions are fairly uniform throughout the cross-section during both tide phases, with the largest values registered in the upper layer during the high tide. The backscatter intensity distributions reveal very small amounts of sediments in this section of the estuary, indicating that most of the particulate matter transported by the river has already settled down.

5 Discussion

5.1 *Exchange flow with the sea*

Given that the variation of the water column height within the harbour zone is negligible compared to the tidal variations, it is assumed that this part of the estuary has a uniform depth varying with time according to the sea level changes. The harbour zone is 12 m deep and has a surface area of about 6×10^5 m^2; therefore, a tidal height difference of the order of 1 m implies that a water volume $V_S \approx 6 \times 10^5$ m^3 enters into (and leaves) it every ($\Delta t =$) 6 h.

In order to estimate the mean velocity u_f of the flow associated with V_S in a simplified way, the volume of exchange water in the shallow part of the estuary is not considered for the moment. According to the description given in Section 4.3, the tidal flow entering the estuary has a cross-section area $A_f \approx 12 \times 200$ m^2 thus implying $u_f = V_S/A_f \Delta t \approx 0.012$ m s^{-1} for the entering current, and a maximum velocity $u_{fm} \approx \pi u_f/2 \approx 0.02$ m s^{-1} if a sinusoidal-like wave is assumed. Note that these values are within the uncertainty interval of the employed ADCPs.

During the ebb tide, the exit of the water volume takes place within the 1 m thick and 200 m wide surface layer, implying a cross-section of $A_e \approx 200$ m^2. This layer reaches a maximum velocity of about 0.24 m s^{-1}, which is 12 times greater than the velocity of the water that entered during the previous tidal stage, consistent with the measured maximum velocities (Fig. 8c and 8d). The mean velocity u_e in this stage is about 0.15 m s^{-1}. In the shallow part of the estuary, velocities are even greater as

illustrated in Fig. 8a. As the water volume exchange with the sea in the harbour zone explains the velocity values found, it is possible to infer that the exchange water volume with the estuarine waters coming from the shallow part is smaller. In such a case, the characteristic times in the harbour zone may be calculated employing the found velocity magnitudes. If V is the total volume of the harbour zone and $Q_f = A_f u_f$, the characteristic time for the sea water to be in the harbour is

$$\tau_{sw} = \frac{V}{Q_f} = \frac{600,000\,\mathrm{m}^2 \times 12\,\mathrm{m}}{2400\,\mathrm{m}^2 \times 0.012\,\mathrm{m\,s}^{-1}} \approx 3\,\mathrm{days} \qquad (3)$$

while the characteristic time for the brackish water that results from the mixing between the sea and freshwater is

$$\tau_{bw} = \frac{V_s}{Q_e} = \frac{600,000\,\mathrm{m}^2 \times 1\,\mathrm{m}}{200\,\mathrm{m}^2 \times 0.15\,\mathrm{m\,s}^{-1}} \approx 5\,\mathrm{h} \qquad (4)$$

where $Q_e = A_e u_e$.

This is valid if the river flow $Q_r < Q_e$. The averaged values of the minimum and maximum river flows are of the order of 10 and 50 $\mathrm{m}^3\,\mathrm{s}^{-1}$, respectively, with extraordinary flows of 200 $\mathrm{m}^3\,\mathrm{s}^{-1}$ or even greater. The velocity distributions reported in Fig. 8 were obtained at reasonably quiet meteorological conditions and with a river flow near the minimum value; hence, the assumptions underpinning the estimates of τ_{sw} and τ_{bw} are reasonable.

Another characteristic time typically calculated for estuaries is the flushing time τ that for the case considered is

$$\tau = \frac{V}{Q_r} = \frac{600,000\,\mathrm{m}^2 \times 12\,\mathrm{m}}{10\,\mathrm{m}^3\,\mathrm{s}^{-1}} \approx 8.3\,\mathrm{days} \quad \text{for } Q_r = 10\,\mathrm{m}^3\,\mathrm{s}^{-1} \qquad (5)$$

and $\tau \approx 1.7$ days for $Q_r = 50\,\mathrm{m}^3\,\mathrm{s}^{-1}$. From these estimates it may be deduced that the whole water in the harbour zone is renewed every 1.7–8.0 days at a given river discharge. However, as explained above, the river freshwater moves in the estuarine surface layer while the layer below is not renewed. Thus, the meaning of the flushing time estimated from the river flow must be revised for this and other similar estuaries, because the deep sea water and the brine surface water have different renewal times.

If $Q_r \leq Q_e$, the surface layer moving towards the sea contains a part $Q_e - Q_r$ of the salt water partly mixed with the fresh water. If $Q_r > Q_e$ at quiet meteorological conditions, the surface layer is expected to be formed only by freshwater. In this case, the river flow dominates and always flows towards the sea over the salt water layer, accelerated or decelerated by the tidal cycles. These results must be further validated in the future studies.

5.2 *Vortices and seiches*

The asymmetry of the exchange flows in the QGRE is caused by the modification of the original morphology due to human action. Hence, particular currents are established which affect the response of the estuarine system to the tides, river flow and sediment transport, as well as to extraordinary events such as sea storms and river floods.

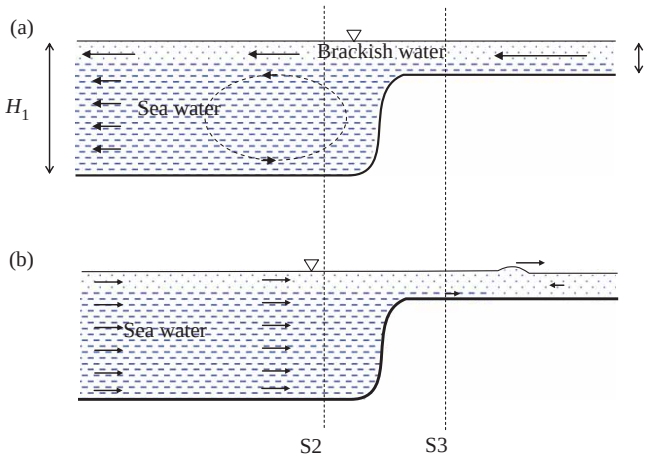

Figure 9 Sketches illustrating the direction of the upper layer, sea water and surface wave during the (a) ebb tide and (b) the flood tide

When the tidal flows are intensified, for example because of strong winds offshore, other phenomena may occur such as those observed during the October 2008 field study. On a vertical plane, the ebb tide generates a weak vortex in the deeper layer of the harbour zone and near the step as illustrated in Fig. 9a. Even though such a vortex was not detected under quiet weather conditions, it is worth noting that the velocities involved are below the resolution limit of the employed measuring instrument; neither has a vortex with opposite rotation direction been detected during the flood tide. Even with intense tidal flows, the sea and brackish waters move with similar velocity throughout the harbour area in this tidal phase. Above the step, a layer of salt water (in the form of a salt wedge) is detected coming into the shallow part of the estuary while a freshwater layer flows in the opposite direction as illustrated by Fig. 4 at S3–S5. On that occasion, a surface wave with amplitude of several tens of centimetres was observed propagating upstream. A possible explanation is that the marine intrusion generates a wave, probably with the characteristics of a bore (Chanson 2009), as shown in Fig. 9b. In this case the velocity of the perturbation was estimated to be 5 $\mathrm{m\,s}^{-1}$ which agrees with the velocity $\sqrt{g\,\langle H\rangle}$ calculated by applying the shallow water approximation, where g is gravity acceleration and $\langle H\rangle$ is the spatially-averaged depth. Later, while the flood tide develops, the whole column of water in the shallow part of the estuary is pushed upstream with increasing velocity.

The rapid variations of the sea level produce standing waves (seiches) generated between a point located in the maritime area (beyond the jetties) and the depth step. The simplified sketch in Fig. 10 helps establish the boundary conditions. The sea fixes a mean height H_1, and a node can be considered to exist there. The sharp change of depth and the smaller width of the bed restrict the flow at the shallow estuary part; therefore the antinode is near the step. If any external factor (such as the rapid change of sea level) provides enough energy, standing waves

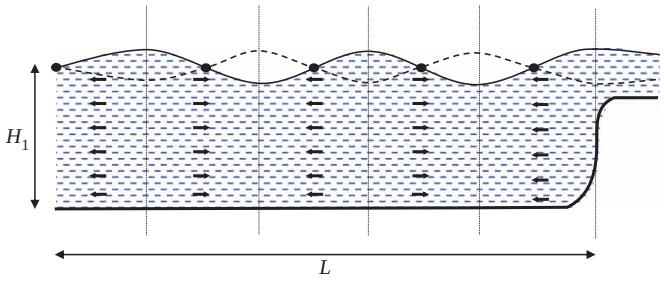

Figure 10 Standing waves in shallow waters modifying the water level (solid line) and velocity (arrows). Points indicate the nodes (constant height sites) and vertical dashed lines represent the anti-nodes (sites where the greatest changes of height are verified). The dashed line suggests the shape of the free surface in the following tidal half-cycle

can be excited between these points. The wavelength λ of the waves is, then, $L/4$, $3L/4$, $5L/4$, etc., where L is the distance between the step and a point located beyond the jetties (in the sea). Assuming the shallow water approximation is valid with the uniform velocity distribution over depth, a succession of regions with the same intensity throughout the water column but with opposite directions along the harbour zone can be deduced.

The distributions of velocity direction and magnitude shown in Fig. 6 and the Fourier analysis of the depth-averaged velocity performed in Section 4.2 support this hypothesis. Naturally, however, the estuarine flows are more complex. The depth step is not exactly an anti-node because it allows a limited flow to and from the shallow part of the estuary. The precise location of the node at the sea is unknown because the estuary mouth is gradual. In addition, the flows in the harbour zone are not exactly one-dimensional (as assumed in Fig. 10), and the forcing may act in a direction that is different from the main estuarine flow.

However, the described simplified model can be useful to identify the key physical processes occurring in this estuary. The standing waves velocity in shallow waters is given by $\sqrt{gH}$, and the period of the anti-nodes maxima and minima is $2\pi\lambda/\sqrt{gH}$. Considering $L \approx 3$ km and $H \approx 12$ m, the periods are of the order of 1 h for the smaller frequencies. As the period of the seiches is shorter than the tidal cycle, the sea level may be considered constant. In addition, the tidal period does not coincide with the period corresponding to any characteristic frequency of the system, so the tide does not excite seiches under normal conditions, and thus the mean height of the free surface in the harbour zone follows the variations of the tidal height. However, upstream of the step the water column height has a mean value that depends on the tide and the amplitude of the generated standing waves (Fig. 10). This suggests that standing waves of extraordinary height might cause waves and floods making the moored boats unstable in the shallow zone as local residents occasionally observe.

5.3 *Sediments dynamics*

As mentioned in Section 3, the bottom sediment is composed mostly of fine sands and coarse silt with mean diameters of about 90 μm, while the fraction of medium and fine silt is minor. The data show that sediments are transported to the harbour in the faster surface layer, which develops on the SW side and covers all the estuary cross-section near the jetties. The flow stops at slack tide and the sediments start to separate from the surface layer to settle on the bottom. During the flood tide, most of the sediments have just settled and the flow velocity in the harbour area is too slow to transport sediments upstream of the step. Thus, the particulate matter is retained in the harbour bed, tending to fill the space artificially created by dredging.

To estimate the size of the particles that settle in the harbour in times of the order of one tidal cycle, let us consider the settling of the individual particles falling to a depth of about 12 m in the time elapsed between two consecutive maxima of the current velocity (≈12 h). Then, the particles should descend with a vertical velocity of 12 m/12 h $\approx 10^{-4}$ m s^{-1}, which is consistent with a grain diameter d of about 20 μm according to the Wentworth chart (Williams *et al.* 2011). The settling velocities of the very fine sands (62.5 μm $< d <$ 125 μm) vary from 0.004 to 0.010 m s^{-1}, descending to the 12 m depth in about 1 h. The existing small fraction of coarse silt (31.25 μm $< d <$ 62.5 μm) settles in just under 4 h, while the sands ($d >$ 125 μm) do it in just under 20 min. These times are shorter than the tidal cycle, and correspond to most of the particle sizes of the bottom sediments in the shallow part. Thus, particles of sand and coarse silt settle in the harbour while fine silt and clay are advected by the currents in the form of wash load. Even if there is no evidence of flocculation, specific analysis of the particles' behaviour is being performed.

In the October 2008 survey, after the sudden rotation of the wind that had been blowing strongly for many hours, intrusions from the surface layer were observed in the distributions of the velocity vertical component (not shown here). Sediments are seen to drop to the bottom more quickly than if particles settled individually. Such intrusions resemble the development of Rayleigh–Taylor instabilities (Sharp 1984) in the interface of an unstable two-layer system in which the upper layer is denser than the lower one. In fact, at rough weather conditions, a strong mixing and more intense currents are found and interfaces are not formed. Such situations are ideal to concentrate great quantities of sediments in the upper layer of the harbour zone due to the drag of the ebb tide. The greater sediment load increases the density of the surface layer and, without a significant salinity or temperature stratification, the favourable conditions to develop the Rayleigh–Taylor instabilities, the generation of intrusions and vertical flows carrying suspended particles to the bottom can be attained. In this case, the convective vertical movements transport all the particles to the bottom regardless of the size. Then fine silt and clay particles have time to drop slowly since the flow velocities are always very low near the bottom. This physical mechanism would explain why there are also fine particles on the harbour bed, although as a small proportion.

With good weather and normal freshwater discharge, the water column is stratified and the conductivity measurements

indicate a salinity in the range $0 < S_1 < 10$ PSU (and consequently, a density $\rho_1 \approx 1000 - 1007\,\mathrm{kg\,m^{-3}}$) in the surface layer, while the lower layer contains pure sea water with salinity $S_2 \approx 34$ PSU (and $\rho_2 \approx 1025\,\mathrm{kg\,m^{-3}}$). The eventual difference of temperature between the layers does not imply a noticeable difference of density. Then, to produce the Rayleigh–Taylor conditions, the denser upper layer must be composed of the suspended particles in a quantity of about $20\,\mathrm{g\,l^{-1}}$. This concentration of suspended particles is too high compared to the measured maximum value ($\sim 0.1\,\mathrm{g\,l^{-1}}$). It is then inferred that the decanting of sediments by means of the mentioned process is unlikely when the stratification is well established and, in fact, such types of intrusions were not detected in field studies performed at good weather.

6 Conclusions

The QGRE flows have undergone significant modifications caused by human intervention. Among other consequences, the deepening and widening of the natural watercourse by dredging generated a decrease of the water velocity and turbulence in the harbour area. Velocity and backscatter intensity measurements, carried out along and across the flow, as well as bathymetric studies were completed to analyse the circulation and sediment dynamics. The findings show that the depth step, in combination with a meander just upstream, induces different circulations in the deep harbour zone and in the shallow part of the estuary, affecting the settling of suspended solids. The local severe storms cause not only an intense tidal intrusion and mixing, but also a stronger ebb flow and seiches when the wind rotates. In addition, the movement of big bulk-carriers and the use of dredgers introduce additional challenges to understanding the estuarine hydrodynamics and the consequent transport and accumulation of sediments (Pereyra 2013).

Acknowledgements

Measurements were carried out with the collaboration of technical staff of the *Instituto Argentino de Oceanografía* (Bahía Blanca, Argentina) and *Centro Internacional de Estudios de Grandes Ríos* (FICH-UNL, Santa Fe, Argentina). The authors thank Dr G. Perillo for his kind collaboration, and the valuable assistance of the JHR Editor.

Funding

This work was financially supported by the Agencia Nacional de Promoción Científica y Tecnológica [grant number 1501/10] and Consejo Nacional de Investigaciones Científicas y Técnicas [grant number 54/10], Argentina.

Notation

A_e	=	cross-section of the surface layer that leaves the estuary during the ebb tide (m^2)
A_f	=	cross-section area of the passage between the jetties during the flood tide (m^2)
d	=	grain diameter (μm)
g	=	gravity acceleration ($m\,s^{-2}$)
H	=	total local depth (m)
H_1	=	sea depth (m)
L	=	distance between the anti-node (step depth site) and the node (located in the sea) (m)
Q_e	=	brackish water outflow during the ebb tide in the harbour zone ($m^3\,s^{-1}$)
Q_f	=	sea water inflow during the flood tide in the harbour zone ($m^3\,s^{-1}$)
Q_r	=	river flow ($m^3\,s^{-1}$)
S	=	salinity (PSU)
u	=	northern component of the velocity averaged in the water column ($m\,s^{-1}$)
u_f	=	mean velocity of the entering current ($m\,s^{-1}$)
u_{fm}	=	maximum velocity of the entering current ($m\,s^{-1}$)
u_e	=	mean velocity of the leaving flow ($m\,s^{-1}$)
V	=	total volume of the harbour zone (m^3)
V_s	=	volume of the surface layer in the harbour zone (m^3)
η_i	=	amplitude of the height wave's i-component of Fourier series expansion (m)
λ	=	waves wavelength (m)
ρ	=	density ($kg\,m^{-3}$)
τ_{sw}	=	characteristic time for the renewal of the sea water in the harbour zone (s)
τ_{bw}	=	characteristic time for the renewal of the brackish water in the harbour zone (s)
τ	=	flushing time (s)
Δt	=	QGRE tidal half-cycle (h)

References

Bale, A.J., Uncles, R.J., Villena Lincoln, A., Widdows, J. (2007). An assessment of the potential impact of dredging activity on the Tamar estuary over the last century: Bathymetric and hydrodynamic changes. *Hydrobiologia* 588(1), 83–95.

Blott, S., Pye, K., Van Der Wal, D., Neal, A. (2006). Long-term morphological change and its causes in the Mersey estuary, NW England. *Geomorphology* 81(1–2), 185–206.

Campo de Ferrera, A.M. (1998). Hidrografia del río Quequén Grande. *PhD Thesis*. Universidad Nacional del Sur, Bahía Blanca, Argentina.

Chanson, H. (2009). Current knowledge in hydraulic jumps and related phenomena. A survey of experimental results. *Eur. J. Mech. B - Fluids* 28(2), 191–210.

Dragani, W.C., Mazio, C.A., Nuñez, M.N. (2002). Sea level oscillations in coastal waters of the Buenos Aires province, Argentina. *Cont. Shelf Res.* 22(5), 779–790.

Dyer, K.R. (1997). *Estuaries: A physical introduction.* Wiley, Chichester.

Franzius Institut fur Grund und Wasserbau der Technische Hoschschule Hannover. (1963). Ensayo sobre modelo hidráulico de Puerto Quequén. *Final Technical Report*, vols. 1–4, Licitación pública 6322, Administración Nacional de Puertos, Buenos Aires, Argentina.

Gan, M.A., Rao, V.B. (1991). Surface cyclogenesis over South America. *Mon. Wea. Rev.* 119(5), 1293–1302.

Gartner, J. (2004). Estimating suspended solids concentrations from backscatter intensity measured by acoustic Doppler current profiler in San Francisco Bay, California. *Mar. Geol.* 211, 169–187.

Guerrero, M., Szupiany, R.N., Amsler, M. (2011). Comparison of acoustic backscattering techniques for suspended sediments investigation. *Flow Meas. Instrum.* 22(5), 392–401.

Isla, F.I., Bértola, G., Merlotto, A., Ferrante, A., Cortizo, L. (2009). Requirements and availability of sand for the protection of Nechochea and Lobería beaches. *Rev. Asoc. Geol. Argent.* 65(3), 446–456.

Lanfredi, N.W., D'Onofrio, E.E., Mazio, C.A. (1988). Variations of the mean sea level in the southwestern Atlantic Ocean. *Cont. Shelf Res.* 8(11), 1211–1220.

Merlotto, A., Piccolo, M.C. (2009). Tendencia climática de Necochea-Quequén (1956–2006), Argentina. *Investigaciones Geográficas* 50, 143–167.

Nichols, M.M., Biggs, R.B. (1985). Estuaries. In *Coastal sedimentary environments.* R.A. Davis, ed. Springer-Verlag, New York, 77–125.

Pari, Y., Ramana Murthy, M.V., Jaya Kumar, S., Subramanian, B.R., Ramachandran, S. (2008). Morphological changes at Vellar estuary, India – Impact of the December 2004 tsunami. *J. Environ. Manage.* 89(1), 45–57.

Parsons, D.R., Jackson, P.R., Czuba, J.A., Oberg, K., Best, J.L., Rhoads, B.L., Engel, F., Riley, J.D. (2013). Velocity mapping toolbox (VMT): A new post-processing suite for acoustic Doppler current profiler data. *Earth Surf. Proc. Landforms* 38(11), 1244–1260.

Pereyra, M.G. (2013). Hydrodynamics of an anthropogenically modified estuary: The Quequén Grande River estuary case. *PhD Thesis.* Universidad Nacional del Centro de la Provincia de Buenos Aires, Tandil, Argentina.

Perillo, G.M.E. (1995). Definition and geomorphologic classifications of estuaries. In *Geomorphology and sedimentology of estuaries, development in sedimentology.* G.M.E. Perillo ed. Elsevier Science BV, Amsterdam, 53, 17–47.

Perillo, G.M.E., Pérez, D.E., Piccolo, M.C., Palma, E.D., Cuadrado, D.G. (2005). Geomorphology and physical characteristics of a human impacted estuary: Quequén Grande River estuary, Argentina. *Estuar. Coast. Shelf Sci.* 62(1–2), 301–312.

Piccolo, M.C., Perillo, G.M.E. (1999). Estuaries of Argentina: A review. In *Estuaries of South America: Their geomorphology and dynamics*. G.M.E. Perillo, M.C. Piccolo, M. Pino Quivira, eds. Environmental Science Series, Springer-Verlag, Berlín, 101–132.

Reeve, D.E., Karunarathna, H. (2009). On the prediction of long-term morphodynamic response of estuarine systems to sea level rise and human interference. *Cont. Shelf Res.* 29(7), 938–950.

Sharp, D.H. (1984). An overview of Rayleigh–Taylor instability. *Physica D* 12(1), 3–18.

Syvitski, J.P.M., Saito, Y. (2007). Morphodynamics of deltas under the influence of humans. *Global Planet. Change* 57(3–4), 261–282.

Van der Wal, D., Pye, K., Neal, A. (2002). Long-term morphological change in the Ribble estuary, Northwest England. *Mar. Geol.* 189(3), 249–266.

Whitham, G.B. (1974). *Linear and nonlinear waves*. John Wiley & Sons, New York.

Williams, J., Arsenault, M.A., Buczkowski, B.J., Reid, J.A., Flocks, J.G., Kulp, M.A., Penland, S., Jenkins, C.J. (2011). Surficial sediment character of the Louisiana offshore continental shelf region: A GIS compilation. Wentworth grain size chart. *United States Geological Survey Open-File Report 1195*.

Wright, R. (1968). Miliolidae (Foraminíferos) recientes del estuario del río Quequén Grande (Buenos Aires). *Hidrobiología* 2(7), 225–256.

Yang, S.L., Ding, P.X., Chen, S.L. (2001). Changes in progradation rate of the tidal flats at the mouth of the Changjiang (Yangtze) River, China. *Geomorphology* 38(1–2), 167–180.